

COMPUTATIONAL STUDY OF STRESS CONCENTRATION ABOUT AN
OBLIQUE HOLE IN A THICK WALLED TUBE: TOWARD UNDERSTANDING
STRUCTURAL IMPROVEMENTS IN BONE

By

SUSAN M. GROVER

A THESIS PRESENTED TO THE GRADUATE SCHOOL
OF THE UNIVERSITY OF FLORIDA IN PARTIAL FULFILLMENT
OF THE REQUIREMENTS FOR THE DEGREE OF
MASTER OF SCIENCE

UNIVERSITY OF FLORIDA

2004

Copyright 2004

by

Susan M. Grover

ACKNOWLEDGMENTS

I would like to thank my husband, Guy Grover, for his emotional support, technical advice, and proofreading. His encouragement has been vital to maintaining the determination necessary to complete the difficult coursework and research required for this degree. His suggestions on finite element modeling techniques helped me to evaluate complex geometries efficiently and accurately.

I would like to express my gratitude to my advisor, Dr. Andrew Rapoff, for his helpful guidance and the concept for this research project. It has been an interesting and rewarding project for me. I am thankful that I was given the opportunity to work on it.

I would like to thank my colleagues in the Applied Biomechanics Laboratory for their support in my research project and in helping to relieve stress. This includes Barbara Garita, Ruxandra Marinescu and Neel Bhatavadekar. Special thanks are in order for Wesley Johnson and Stephanie Dudley, both former students in the Applied Biomechanics Laboratory who convinced me to join Dr. Rapoff's group of graduate students. It has been a very satisfying experience for me and I am forever grateful.

I would also like to thank my parents, Julian and Sue Mathison, for encouraging me to go back to school after five years of work and being supportive of me. Their confidence in me and enthusiastic encouragement since childhood have enabled me to accomplish all of my goals thus far.

TABLE OF CONTENTS

	<u>page</u>
ACKNOWLEDGMENTS	iii
LIST OF TABLES	vi
LIST OF FIGURES	vii
ABSTRACT	ix
NOTATION	viii
CHAPTER	
1 INTRODUCTION	1
2 BACKGROUND	3
3 FINITE ELEMENT MODELS	7
4 RESULTS	15
Generation of Results	15
Listing of Results	16
Validation: Cylinders with Transverse Holes	18
Validation: Flat Plates with Oblique Holes	19
Angle of Obliquity, α	20
Hole Size Ratio, d/D	22
Cylinder Diameter Ratio, d_i/D	24
Angular Location of Maximum Stress, θ	25
Depth of Maximum Stress in Hole, h	27
Angle of Neutral Axis, ψ	29
5 DISCUSSION	30
Angle of Obliquity, α	30
Hole Size Ratio, d/D	31
Cylinder Diameter Ratio, d_i/D	32
Angular Location of Maximum Stress, θ	32
Depth of Maximum Stress in Hole, h	33

Angle of Neutral Axis, ψ	33
6 CONCLUSIONS	35
LIST OF REFERENCES.....	38
BIOGRAPHICAL SKETCH	39

LIST OF TABLES

<u>Table</u>	<u>page</u>
3-1 Model listing	9
4-1 Maximum and minimum stress concentration factors, with location	17

LIST OF FIGURES

<u>Figure</u>	<u>page</u>
3-1 Cylinder parameters (forces shown at $\psi = 0^\circ$).....	8
3-2 Hole parameters.....	8
3-3 Sketch of 10-node parabolic tetrahedral element.....	10
3-4 Volume partitions, volume labels circled.....	12
4-1 Comparison of results from FEA and Pilkey [2].....	19
4-2 Comparison of results from FEA and Stanley and Day [5]	20
4-3 K_{max} plotted against α	22
4-4 K_{min} plotted against α	23
4-5 K_{max} plotted against hole size ratio, d/D , at $d_i/D = 0.75$	24
4-6 K_{min} plotted against hole size ratio, d/D , at $d_i/D = 0.75$	24
4-7 K_{max} plotted against d_i/D for various α at $d/D = 0.10$	25
4-8 K_{min} plotted against d_i/D for various α at $d/D = 0.10$	25
4-9 Angular location of K_{max} , θ , plotted against α	26
4-10 Normalized depth of K_{max} in the hole interior plotted against α	28

NOTATION

d	hole diameter
d_i	cylinder inner diameter
D	cylinder outer diameter
F	applied force (N)
h	normalized depth in the hole, measured from the mid-plane
K_{max}	maximum stress concentration factor based on the gross cross section, $\sigma_{max}/\sigma_{nom}$
K_{min}	minimum stress concentration factor based on the gross cross section, $\sigma_{min}/\sigma_{nom}$
r	radial location, used to identify the location of K_{max} and K_{min}
t	cylinder wall thickness
z	height coordinate ($z = 0$ is at the fully restrained end of the cylinder)
α	angle of obliquity, i.e. angle the hole centerline makes with a vector normal to the surface of the cylinder ($^\circ$)
θ	clock position around the hole, measured in the plane perpendicular to the hole centerline from the point farthest from the direction of applied load ($^\circ$)
θ'	clock position around the hole, measured in a plane parallel to the cylinder surface from the point farthest from the direction of applied load ($^\circ$)
ψ	angular location of the neutral axis from a datum line oriented perpendicular to the hole axis ($^\circ$). (At $\psi = 0^\circ$, the region of material around the hole is in tension)
σ_{max}	maximum principal stress at a point sufficiently distant from the applied load
σ_{min}	minimum principal stress at a point sufficiently distant from the applied load
σ_{nom}	nominal stress in a body without a discontinuity

Abstract of Thesis Presented to the Graduate School
of the University of Florida in Partial Fulfillment of the
Requirements for the Degree of Master of Science

COMPUTATIONAL STUDY OF STRESS CONCENTRATION ABOUT AN
OBLIQUE HOLE IN A THICK WALLED TUBE: TOWARD UNDERSTANDING
STRUCTURAL IMPROVEMENTS IN BONE

By

Susan M. Grover

August 2004

Chair: Andrew J. Rapoff
Major Department: Biomedical Engineering

To quantify improvements in stress in the canine tibia near the nutrient foramen (a natural hole) the expected stress concentration factor around a similar hole in a homogenous isotropic structure is needed for comparison purposes. The canine tibia is loaded in bending and includes a foramen oriented at an oblique angle to the long axis. This loading and geometry have been somewhat neglected in previous stress concentration factor research, though experimental and computational results exist for flat plates with oblique holes in tension and cylinders with transverse holes in either tension or bending.

A series of finite element models have been created to investigate stress concentration factors in homogeneous isotropic hollow cylinders in bending with holes ranging from transverse to oblique. The results of this parametric study indicate that, as the hole becomes more sharply angled, both the maximum and minimum stress

concentration factors decrease and shift toward the acutely angled edge created by the intersection of the hole with the cylinder surface.

This study includes minimum stress concentration factors, which were largely unreported in prior work, but are very important to this investigation. Due to loading differences, the absolute value of these factors should be compared to maximum stress concentration factors occurring in the canine tibia. This comparison can be used to help quantify the ability of bone to reduce stress around a natural discontinuity.

CHAPTER 1 INTRODUCTION

Localized stress around geometric discontinuities such as holes, shoulders, and grooves cannot be predicted using elementary stress formulas. The concentration of stress resulting from these abrupt transitions is frequently too high to be attributed solely to the decrease in net cross sectional area. Stress concentration factors, often determined experimentally or computationally, are used to scale the nominal stress in a continuous structure to account for the effect of the discontinuity.

Determining stress concentration factors is of practical importance for many engineered structures because geometric discontinuities are frequently the site of failure, but, in bone, this is not always the case. Although surgically created holes may be a source of failure, natural holes, such as the nutrient foramen, seem to demonstrate superior mechanical performance. Modifications in porosity, mineralization, and fiber orientation can work together to decrease stiffness around a discontinuity to reduce stress. A unique microstructure was previously uncovered at the equine third metacarpus nutrient foramen that results in an elimination of stress concentration at the hole edge, i.e. the structure behaves as if it were continuous [1].

When compared to the expected stress concentration in a homogeneous isotropic structure, the effect of the geometry and microstructure of the hole can be quantified. The nutrient foramen in the equine third metacarpus is oriented normal to the surface of the bone. The hole is elliptically shaped with an aspect ratio of approximately 2:1 [1]. The major axis is parallel to the long axis of the bone and the bone is loaded primarily in

uniaxial compression. The expected stress concentration factor for a circular hole in a homogeneous isotropic infinitely large plate with uniaxial stress is 3.00 [2]. Elongating the hole such that the major axis of the ellipse is parallel to the line of action of the load and the aspect ratio is 2:1 results in an expected stress concentration factor of 2.00 in a homogeneous isotropic structure [2]. The microstructure in bone, then, is responsible for reducing the stress concentration factor further to 1.00 [1].

The effect of the geometry and microstructure around a nutrient foramen oriented and shaped differently could provide more insight into the ability of bone to reduce stress. The canine tibia includes a nutrient foramen that enters the bone at a steep angle. This bone is subjected to bending in the saggital plane and the nutrient foramen is located on the posterior surface, in a region subjected primarily to compression. The stress field for this geometry is more complex than that of a flat plate in uniaxial loading. The maximum stress depends on many factors, including the angle of obliquity, the wall thickness, and the ratio of the hole diameter to the outer diameter of the cylinder.

A literature review has not revealed a prior investigation of stress concentration factors for oblique holes in cylinders. The ensuing discussion will provide a set of results that can be used to predict stress concentration factors for homogeneous, isotropic, linearly elastic cylinders with oblique holes. This can later be used to form a comparison with the stress concentration factors predicted through a microstructural examination of the canine tibia to quantify the change in stress concentration achieved by bone.

CHAPTER 2 BACKGROUND

Considerable prior work has focused on predicting stress concentration factors for flat plates with oblique holes and for cylinders with transverse holes, but the combined effect of an oblique hole in a cylinder seems to be a neglected area of study. An investigation into this overlooked geometry, however, can shed light on variations in stress near the hole when the angle of obliquity, wall thickness, and hole diameter change and provide a set of results to compare to stress concentration factors in various bones near foramina.

The microstructural analysis detailed in Götzen et al. [1] demonstrates a method for determining heterogeneous anisotropic elastic constants in bone using porosity, mineralization, fiber orientation, and osteon orientation measurements. A finite element model was created using a geometry that closely matches that of bone. The elastic constants were mapped to appropriate locations in the model to simulate the mechanical variations that occur in bone. Loading this model in a manner similar to physiological loading revealed the stress pattern that would be expected in vivo. From this, the stress concentration factor was calculated. In the equine third metacarpus study, this factor is 1.00 [1].

In one of the earliest works on oblique holes in flat plates, Ellyin, Lind, and Sherbourne [3] developed a theoretical solution for thin plates with holes between 0° and 45° of obliquity, as measured from a vector normal to the surface of the plate (see α in Figure 3-2). The solution was obtained by dividing the plate into several thin membranes

and enforcing plane elasticity, maintaining compatibility by applying tractions at the boundary surfaces. The results demonstrated that as Poisson's ratio increases, the stress concentration factor decreases. Also, for holes loaded in uniaxial tension parallel to the minor axis of the ellipse created at the hole surface, the maximum stress concentration factor (located near the major axis) increases as the obliquity increases. This analytical approach provided a basis for future work in this area.

The results of the theoretical work seemed to agree fairly well with Ellyin's later experimental study [4], which involved affixing strain gauges to steel plates with holes of varying obliquity, diameter, and load orientation (parallel to either the major or minor axis of the ellipse). A limitation of this method, mentioned by Ellyin [4], results from the difficulty in recording accurate strain measurements in regions with high strain gradients. Since strain gradients tend to increase with hole obliquity, this limits the useful range of obliquities that can be adequately studied with this method.

Ellyin's results demonstrate trends for both load orientations investigated. For holes loaded parallel to the minor axis of the ellipse, K_{max} rises rapidly as obliquity steadily increases. The opposite is true for holes loaded parallel to the major axis; i.e., for these holes, K_{max} decreases rapidly as obliquity steadily increases. For either hole orientation, as obliquity increases from 0° to 45° (i.e. as the hole becomes steeper), the location of maximum strain (and stress) moves from the mid-plane of the plate toward the plate surface [4]. Ellyin measured the location of stress inside the hole by applying at least five strain gauges every 45 degrees around the circumference of the hole, spaced at equal distances throughout the thickness.

Stanley and Day [5] were among the first to consider applied loads oriented at various angles from 0° to 90° with respect to the major axis of the ellipse. As expected based on Ellyin's results [4], the stress concentration factor increased as the angle of load application was varied from parallel to the major axis of the ellipse to parallel to the minor axis. The results also confirm that, when the load is applied parallel to the minor axis, as the obliquity angle increases, the stress concentration factor increases and shifts from mid-plane (at a 0° angle of obliquity) to the plate surface (at a 60° angle of obliquity). Conversely, when the applied load is parallel to the major axis, as the obliquity angle increases, the stress concentration factor decreases and stays close to the mid-plane for all obliquity angles less than 60° .

The most comprehensive work to date on oblique holes in flat plates is Dulieu-Barton and Quinn's thermoelastic study [6]. The variable definitions used are the same as those chosen for Stanley and Day's photoelastic study [5], but the plate thickness-to-hole diameter ratios were smaller. The results revealed that, similar to the findings of Stanley and Day [5], when the applied tensile load is parallel to the minor axis of the surface ellipse, increasing the obliquity angle causes increased maximum stress values. An important observation of the study is that, for the thickness-to-hole diameter ratios considered, as this ratio decreases, the stress concentration factor increases. This confirms the findings of Ellyin [4] and Daniel [7], while disputing the weak dependency reported by Stanley and Day [5].

Hollow cylinders with transverse holes through one or both walls have been studied in tension, bending, or torsion in Jessop et al. [8] and results have been summarized in Pilkey [2]. The results of the photoelastic study in Jessop et al. [8] indicate that, for the

tensile loading case, stress concentration factors decrease as the hole diameter-to-outer cylinder diameter ratio increases and wall thickness decreases. For the bending load case, however, Jessop et al. [8] demonstrates that as the hole diameter-to-outer cylinder diameter ratio increases, the stress concentration factor first decreases slightly and then increases more sharply.

The effects of varying the wall thickness and the hole diameter were also uncovered by Jessop et al. [8]. It was also shown that, as wall thickness decreases, maximum stress concentration increases slightly. Varying the hole diameter had a greater effect on the stress concentration factor than changing the cylinder diameter ratio, so the size of the hole has more of an influence than wall thickness on the stress concentration factor [8].

The project documented herein will investigate stress concentration factors in hollow cylinders with oblique holes in bending. Magnitude and location of both minimum and maximum stress concentration factors will be reported at various obliquity angles, hole diameters, and wall thicknesses. The location of the maximum principal stress will be reported in terms of angular location and normalized distance from the mid-plane. Plots of all data will be presented and compared to prior work, when applicable.

CHAPTER 3 FINITE ELEMENT MODELS

Finite element models were created using SDRC I-DEAS MS-9 software on a Windows 2000 based PC. The parameters used in this study are illustrated in Figure 3-1 and Figure 3-2. All parameter combinations used in this investigation are listed in Table 3-1. The parameters chosen for each model were selected such that hole diameter, angle of obliquity and wall thickness may be studied in isolation of the other parameters.

All models were fully restrained in all six degrees of freedom at the $z = 0$ end and a bending load was applied at the opposite end. Cylinder heights were chosen such that the constraints and loads are located at a distance of at least 3 times the maximum cylinder diameter away from the hole to minimize any effect that the manner of loading may have on the stress at the hole.

The bending load was generated using two point forces. A 100 Newton tensile force was applied on a node located directly above the hole center at a radial location, r , of $D/2$ and a 100 Newton compressive force was applied on a node located 180° away, also at $r = D/2$. The angular location of the neutral axis from a datum line oriented perpendicular to the hole axis is designated by ψ . For the loading pattern described and used for all models herein, ψ is zero. This load puts the hole region in tension.

The variable θ was created to facilitate a direct comparison of the angular location of maximum stresses in each model. This is defined as the angular position around the circular hole and is used in favor of θ' , which is defined as the angular position around

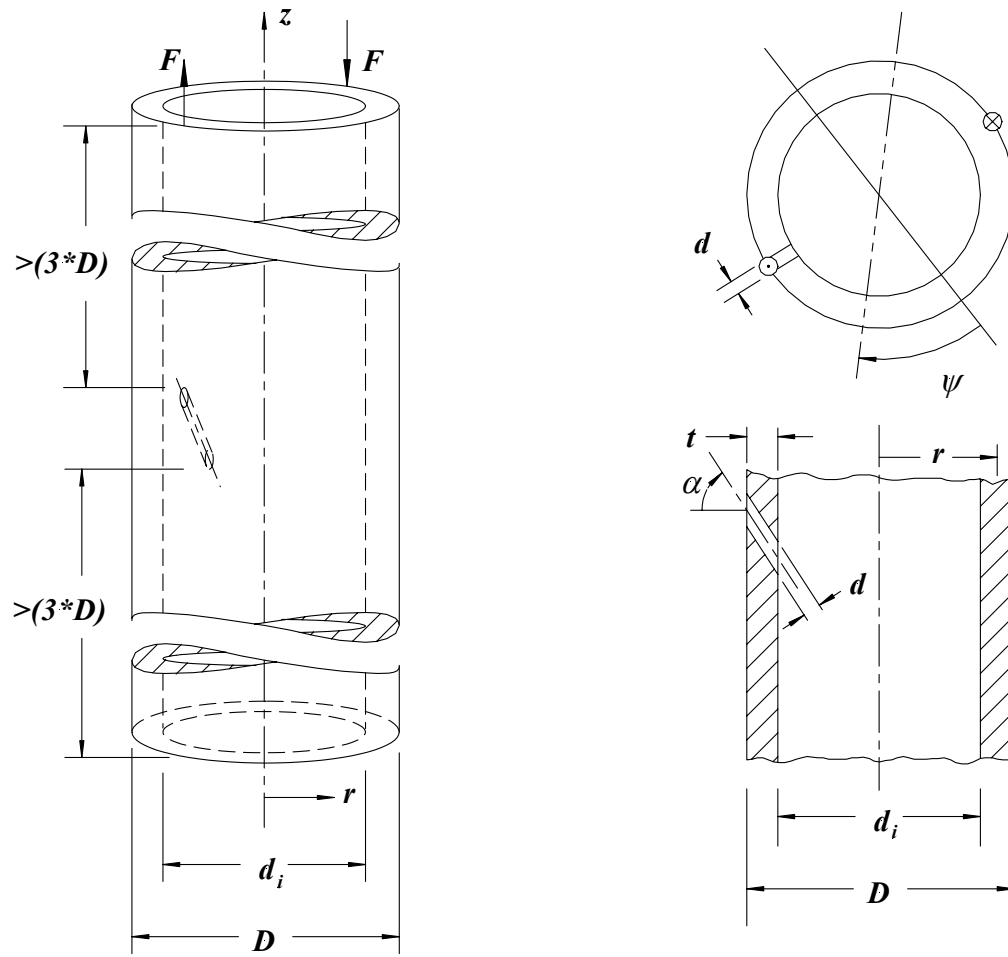


Figure 3-1 Cylinder parameters (forces shown at $\psi = 0^\circ$)

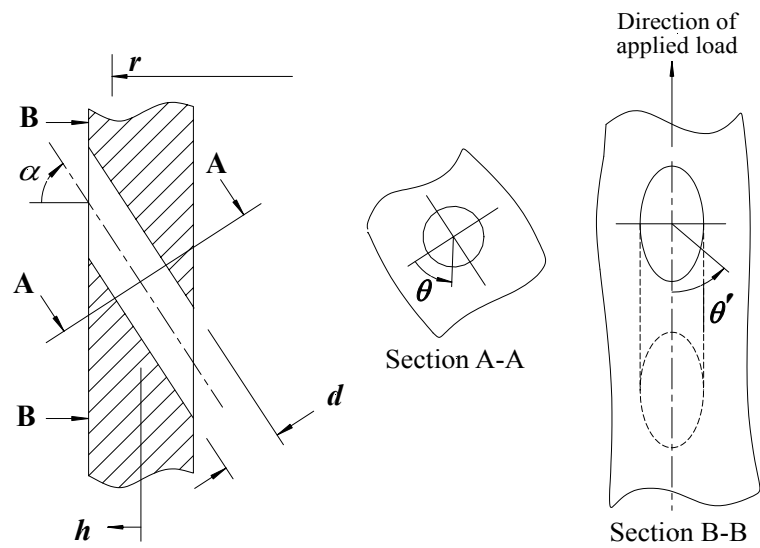


Figure 3-2 Hole parameters

Table 3-1 Model listing

Model	d (mm)	α (deg.)	D (mm)	d_i (mm)	d_i/D
1	1	0	20	5	0.25
2	1	0	20	10	0.5
3	1	0	20	15	0.75
4	2	0	20	5	0.25
5	2	0	20	10	0.5
6	2	0	20	15	0.75
7	3	0	20	5	0.25
8	3	0	20	10	0.5
9	3	0	20	15	0.75
10	1	15	20	5	0.25
11	1	15	20	10	0.5
12	1	15	20	15	0.75
13	2	15	20	5	0.25
14	2	15	20	10	0.5
15	2	15	20	15	0.75
16	3	15	20	5	0.25
17	3	15	20	10	0.5
18	3	15	20	15	0.75
19	1	30	20	5	0.25
20	1	30	20	10	0.5
21	1	30	20	15	0.75
22	2	30	20	5	0.25
23	2	30	20	10	0.5
24	2	30	20	15	0.75
25	3	30	20	5	0.25
26	3	30	20	10	0.5
27	3	30	20	15	0.75
28	1	45	20	5	0.25
29	1	45	20	10	0.5
30	1	45	20	15	0.75
31	2	45	20	5	0.25
32	2	45	20	10	0.5
33	2	45	20	15	0.75
34	3	45	20	5	0.25
35	3	45	20	10	0.5
36	3	45	20	15	0.75
37	1	60	20	5	0.25
38	1	60	20	10	0.5
39	1	60	20	15	0.75
40	2	60	20	5	0.25
41	2	60	20	10	0.5
42	2	60	20	15	0.75
43	3	60	20	5	0.25
44	3	60	20	10	0.5
45	3	60	20	15	0.75
46	1	75	20	5	0.25
47	1	75	20	10	0.5
48	1	75	20	15	0.75
49	2	75	20	5	0.25
50	2	75	20	10	0.5
51	2	75	20	15	0.75
52	3	75	20	10	0.5
53	3	75	20	15	0.75

the ellipse on the cylinder surface. This notation, illustrated in Figure 3-2 is consistent with that used by in refs. [5], [6], and [9].

All nodes and elements were created using the free mesh option in I-DEAS, which uses solid tetrahedral elements. Quadratic tetrahedral elements were selected over linear tetrahedrons because the former elements provide more accurate displacement results and, hence, more accurate stress results for structures exhibiting a displacement field that is not linear. Linear tetrahedrons can only achieve linear displacement and constant stress and strain within the element [10].

Parabolic tetrahedral elements are identified as element type 118 in I-DEAS. They include four corner nodes and six midside nodes. Three translational degrees of freedom are allowed at each node, such that parabolic deformation of each edge is permitted [11]. The displacements of this element are defined by a set of complete quadratic polynomials, specified in Cook et al. [10]. This enables these elements to represent a quadratic displacement field within the element. Four integration points are used for these elements. Nodal stresses and strains are extrapolated from the values at the integration points [11]. Figure 3-3 is a sketch of this element and the associated nodes.

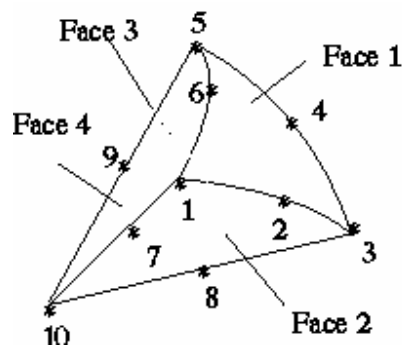


Figure 3-3 Sketch of 10-node parabolic tetrahedral element

The automatic mesh checking function in I-DEAS was used to enforce the condition that the elements generated have a distortion value greater than 0.1 and a stretch value greater than 0.2. The I-DEAS User's Guide suggests that distortion or stretch above 0.05 is usually acceptable for tetrahedral elements [11]. An ideal element, i.e. a straight-sided tetrahedron with mid-side nodes located in the geometric center of each line with equilateral triangular faces, would have distortion and stretch values of 1.00. Preventing excessive distortions allows these elements to more accurately represent high order displacement modes [10].

To decrease the number of elements required, each cylinder was partitioned into five volumes prior to meshing. The mesh density generally decreased as the distance from the thru-hole increased. The five volumes, illustrated in Figure 3-4, include two concentric volumes surrounding the hole, with maximum diameters of three and five times the diameter of the hole, labeled as volumes 1 and 2, respectively. A central volume encompasses most of the cylinder and is labeled as volume 3. Upper and lower cylindrical volumes with heights that are 1/5 of the total height are labeled as volumes 4 and 5.

Material properties applied to the models were selected to be as general as possible, maintaining linear elastic behavior, isotropy, and homogeneity. Properties provided by SDRC I-DEAS for generic isotropic steel were used. The elastic modulus is 206,800 N/mm², Poisson's ratio is 0.29, and shear modulus is 80155 N/mm².

Model 1 in Table 3-1 was selected for a convergence study. This geometry was chosen because it will require the maximum number of elements around the hole to attain convergence. All other models were created using the converged mesh density

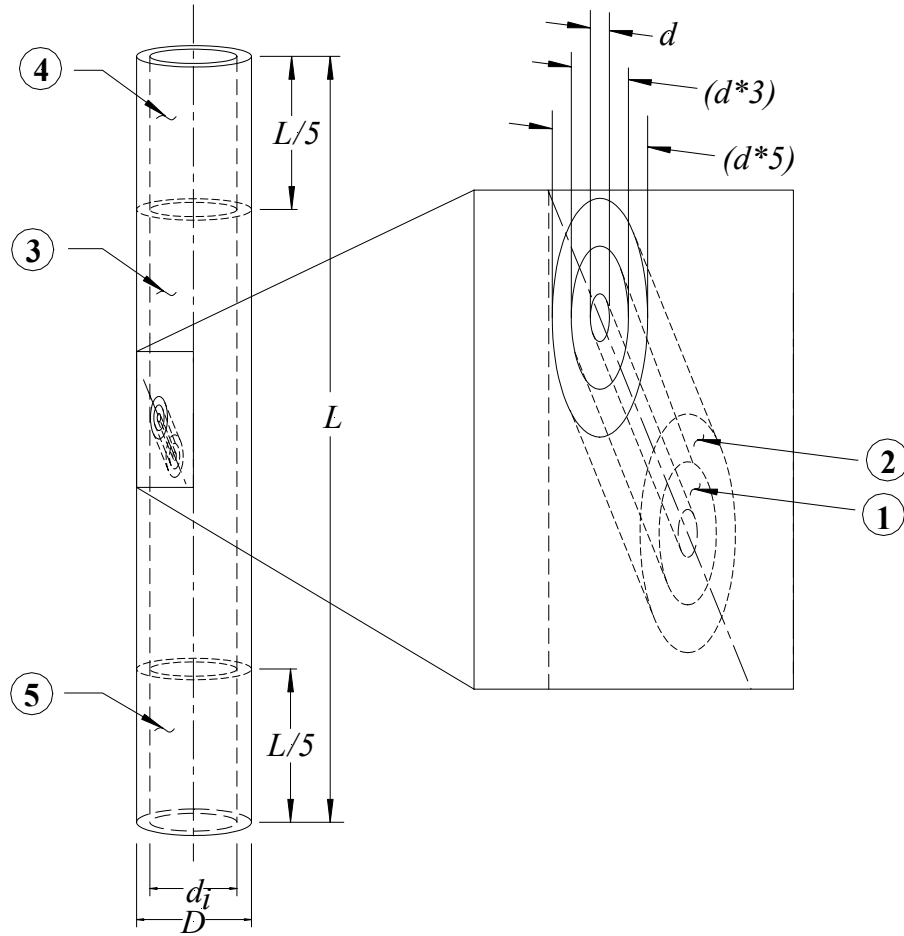


Figure 3-4 Volume partitions, volume labels circled

determined from this model. Parameters for this model include an outer diameter of 20 mm, an inner diameter of 15 mm, a hole diameter of 1 mm, and an obliquity angle of 75° . This represents the thinnest wall, smallest hole, and largest angle of obliquity.

Models with smaller obliquity angles would likely converge sooner and require a less dense mesh because they would be less prone to have geometric issues such as sharp angles and thin walls that generally require smaller elements to achieve convergence. The additional time required to solve all models with a finer mesh was acceptable compared to the time required to perform a convergence study on each model.

An initial attempt at stress convergence provided inconclusive results because a large stress gradient is present for large obliquity angles. An inconsistent placement of nodes between models with varying mesh densities was identified as the problem. The free mesh generated in I-DEAS results in a non-uniform nodal placement, so the exact location of maximum stress varied slightly from mesh to mesh.

To resolve this problem, the convergence study was repeated after investigating the location of maximum stress. The seven meshes created for location investigation used specified element lengths between 0.16 and 0.28 millimeters in volume 1. The average angular location of maximum stress concentration around the ellipse was $\theta' = 7.92^\circ$ (± 0.79 SD). The percent standard deviation on the location of maximum stress is less than 10 percent, so, in models created after the conclusion of the convergence study, an investigation into the location of maximum stress was not performed. It is assumed that, by using a consistent mesh density equal to the converged mesh density for model 1, the location and magnitude of maximum stress in later models will be accurate.

Four finite element meshes were used to test for convergence. In each of the meshes used for the convergence study, two nodes were generated on the elliptical intersection of the hole and the cylinder surface at $\theta' = \pm 7.92^\circ$. Figure 3-5 shows the variation in maximum stress at the two pre-set node locations as mesh density is increased. Convergence begins to occur when approximately 29000 elements are used for volume 1, corresponding to a specified element length (equivalent to the cube root of the element volume) of 0.22 millimeters. In the other volumes, specified element lengths are progressively larger as the distance from the thru-hole increases. The number of elements used in the models ranged from 66997 to 428027 elements.

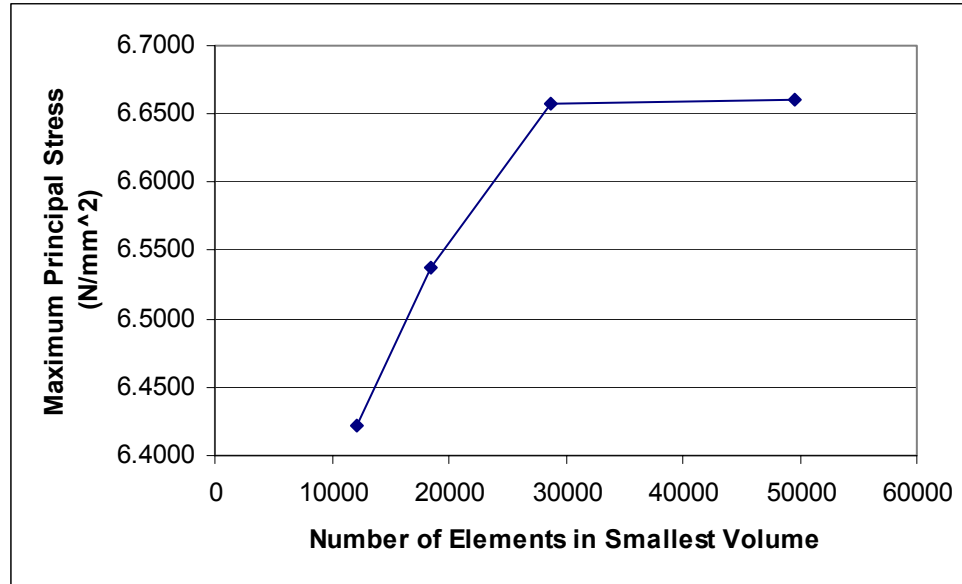


Figure 3-5 Maximum stress plotted against number of elements in volume 1

CHAPTER 4 RESULTS

Generation of Results

Maximum and minimum stress concentration factors are calculated using a ratio of the maximum or minimum principal stress to a nominal value, as shown below.

$$K_{max} = \frac{\sigma_{max}}{\sigma_{nom}}$$

$$K_{min} = \frac{\sigma_{min}}{\sigma_{nom}}$$

The variables σ_{max} and σ_{min} are the maximum and minimum principal stress, respectively, in volume 1, the smallest volume that encompasses the hole.

The nominal stress, σ_{nom} , may be defined using either the gross cross sectional area or the net cross sectional area. There are advantages to both approaches. To predict stress using the gross cross section approach, a stress value is initially calculated without considering the hole. This value is then scaled by the gross stress concentration factor. A stress concentration factor calculated based on the gross cross section accounts for the combined effects of a reduction in cross sectional area and the stress concentration effect.

The net cross sectional area results in a more precise representation of the stress concentration effect of the hole. However, it is less practical, since it requires calculating the stress using the reduced cross section before applying the factor to predict maximum stress. If the hole size is sufficiently small such that the decrease in cross-sectional area is minimal, the gross cross-sectional stress may be used with little sacrifice to precision.

The reference stress, σ_{nom} , is calculated as shown below using the flexure formula, where S is the section modulus.

$$\sigma_{nom} = \frac{F(D)}{S}$$

The section modulus is a ratio of the moment of inertia to the distance of the applied load from the neutral axis. For a continuous hollow cylinder (with no discontinuity),

$$S = \frac{\pi}{32} \left(\frac{D^4 - d^4}{D} \right)$$

Pilkey [2] suggests that for a flat plate, if the hole diameter-to-plate width ratio is less than 0.5, the gross cross sectional stress may be used. The cylinders used for this study fit within these parameters. In fact, for the geometries used in this study, the cross sectional area decreases a maximum of 8 % after the hole area is removed, so the nominal stress for this study is based on the gross cross section.

Listing of Results

Maximum and minimum stress concentration factors near the hole are listed in Table 4-1. Also included are the position (radial, r , and angular, θ) of the maximum and minimum stress concentration factors. Results were obtained using the I-DEAS solver and post-processor. Maximum and minimum principal stresses occur exclusively on the hole surface, located either on the hole interior or at the intersection of the hole with the cylinder surface.

There is a center of symmetry for oblique holes, such that for each point on the hole there is a corresponding point at which the stress state is identical. Due to the non-uniform placement of nodes in this study, however, the resulting stress values at

Table 4-1 Maximum and minimum stress concentration factors, with location

Hole Details				Max. Stress Concentration Factor, K_{max}			Min. Stress Concentration Factor, K_{min}		
Model	α ($^{\circ}$)	d/D	d_i/D	Value	θ ($^{\circ}$)	r	Value	θ ($^{\circ}$)	r
1	0	0.05	0.25	2.94	92.59	9.40	-0.956	-179.40	9.62
2	0	0.05	0.5	2.95	85.53	9.32	-0.998	-176.45	9.53
3	0	0.05	0.75	3.00	94.36	9.71	-1.051	1.03	9.51
4	0	0.1	0.25	2.96	-90.60	9.69	-0.963	-179.42	8.89
5	0	0.1	0.5	2.97	92.26	9.71	-0.977	-178.30	9.01
6	0	0.1	0.75	3.02	88.43	9.54	-1.041	-177.51	8.93
7	0	0.15	0.25	2.97	-91.08	9.60	-0.943	-1.88	8.63
8	0	0.15	0.5	2.96	-92.91	9.58	-0.966	179.57	8.70
9	0	0.15	0.75	3.03	92.26	9.54	-1.050	-0.09	8.62
10	15	0.05	0.25	2.91	82.63	9.71	-1.061	-6.57	9.83
11	15	0.05	0.5	2.90	73.79	9.52	-1.037	-3.68	9.60
12	15	0.05	0.75	2.86	66.72	9.30	-1.087	-2.17	9.67
13	15	0.1	0.25	2.88	81.60	9.60	-1.040	0.21	9.65
14	15	0.1	0.5	2.86	82.89	9.69	-1.038	-2.01	9.46
15	15	0.1	0.75	2.91	80.84	9.62	-1.067	-1.06	9.24
16	15	0.15	0.25	2.88	80.07	9.41	-1.031	2.23	9.20
17	15	0.15	0.5	2.91	-81.07	9.56	-1.046	-1.15	9.26
18	15	0.15	0.75	2.95	-80.59	9.73	-1.186	178.59	7.50
19	30	0.05	0.25	2.63	-72.63	9.90	-1.186	4.23	9.93
20	30	0.05	0.5	2.64	68.34	9.71	-1.078	7.38	10.00
21	30	0.05	0.75	2.69	65.07	9.70	-1.141	-5.29	10.00
22	30	0.1	0.25	2.64	-74.05	9.70	-1.161	1.64	9.86
23	30	0.1	0.5	2.65	72.18	9.70	-1.197	-1.26	9.92
24	30	0.1	0.75	2.70	72.59	9.69	-1.309	5.26	7.50
25	30	0.15	0.25	2.68	72.56	9.70	-1.137	-0.28	9.62
26	30	0.15	0.5	2.69	76.66	9.90	-1.144	-0.86	9.85
27	30	0.15	0.75	2.76	76.35	9.91	-1.531	169.60	7.50
28	45	0.05	0.25	2.38	-69.07	10.00	-1.502	-4.18	10.00
29	45	0.05	0.5	2.36	-69.07	10.00	-1.494	-4.18	10.00
30	45	0.05	0.75	2.35	-69.09	10.00	-1.541	-4.18	10.00
31	45	0.1	0.25	2.41	66.09	10.00	-1.554	2.34	10.00
32	45	0.1	0.5	2.41	66.09	10.00	-1.558	2.34	10.00
33	45	0.1	0.75	2.47	66.08	10.00	-1.736	-0.26	7.50
34	45	0.15	0.25	2.48	-63.54	10.00	-1.494	-0.41	10.00
35	45	0.15	0.5	2.50	65.83	10.00	-1.499	-3.93	10.00
36	45	0.15	0.75	2.56	68.32	10.00	-1.993	-3.67	7.50
37	60	0.05	0.25	2.08	48.86	10.00	-1.807	-2.93	10.00
38	60	0.05	0.5	2.07	48.86	10.00	-1.794	-2.93	10.00
39	60	0.05	0.75	2.10	48.86	10.00	-1.811	-2.93	10.00
40	60	0.1	0.25	2.14	52.00	10.00	-1.928	-1.87	10.00
41	60	0.1	0.5	2.16	52.00	10.00	-1.960	-1.87	10.00
42	60	0.1	0.75	2.23	52.00	10.00	-2.196	-0.68	7.50
43	60	0.15	0.25	2.22	48.82	10.00	-1.937	2.21	10.00
44	60	0.15	0.5	2.25	-51.16	10.00	-1.959	2.21	10.00
45	60	0.15	0.75	2.31	-51.17	10.00	-2.688	-0.30	7.50
46	75	0.05	0.25	1.73	-29.61	10.00	-1.439	0.01	10.00
47	75	0.05	0.5	1.72	30.66	10.00	-1.372	-0.04	10.00
48	75	0.05	0.75	1.78	31.22	10.00	-1.273	-4.90	10.00
49	75	0.1	0.25	1.82	-28.42	10.00	-2.056	-2.21	10.00
50	75	0.1	0.5	1.84	27.79	10.00	-2.047	-2.21	10.00
51	75	0.1	0.75	1.93	-28.29	10.00	-2.112	-1.93	7.50
52	75	0.15	0.5	1.94	-30.42	10.00	-2.383	-0.07	10.00
53	75	0.15	0.75	2.02	30.35	10.00	-3.587	1.46	7.5

symmetrical points are not exactly the same. The position indicated in the table is the location where the maximum or minimum principal stress occurs.

The angular coordinate θ' listed in Table 4-1 is calculated directly from the coordinates of the node of interest (see Figure 3.2). This angle is transposed into the θ -plane for direct comparison of the position of maximum stress between cylinders with varying angles of obliquity. Both angles are equal to zero at the position farthest from the direction of the applied load. The relationship between θ' and θ is

$$\tan \theta' = \tan \theta \cos \alpha$$

Validation: Cylinders with Transverse Holes

A photoelastic study performed by Jessop, Snell and Allison [8], which produced stress concentration factors for cylinders with a transverse hole extending through both walls subjected to tension, bending, or torsion, is the most applicable prior work for comparison to this study. The results of the bending tests were fitted to a polynomial expression in Pilkey [2]. Figure 4-1 is a plot of K_{max} against the hole size ratio, d/D , for $\alpha = 0$ from the current study and from the photoelastic results expressed in Pilkey [2] for a cylinder in bending. In each configuration, the finite element results exceed the experimental values. The maximum percent difference between the FEA results and the photoelastic results is 8.2 % at $d/D = 0.10$ and $d_i/D = 0.25$.

It is important to note that the results from Pilkey [2] are based on a cylinder with a transverse hole extending through the cylinder, whereas the current study considers a hole through the wall only. An additional finite element model was created based on the model geometry identified as having the maximum percent difference, but modified with the addition of a transverse hole in the opposite wall. K_{max} from this model, identified as

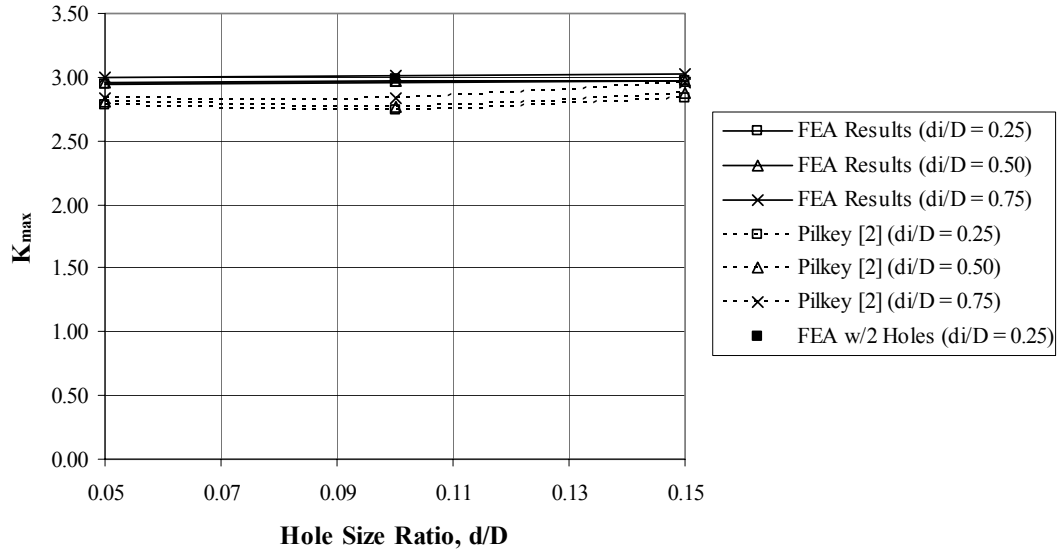


Figure 4-1 Comparison of results from FEA and Pilkey [2]

‘FEA w/2 Holes’ is marked as a solid black square in Figure 4-1. A comparison of this result to the applicable geometry in Pilkey [2] reveals an 8.8 % difference. Tafreshi and Thorpe [9] compared finite element analysis results of a plate in tension to photoelastic results of a plate in tension and reported 8.9 % difference between photoelastic and finite element results, so *the current percent difference is within expected levels*. The low percent difference is an indication that the finite element analysis results compare well to experimental results.

Validation: Flat Plates with Oblique Holes

A further investigation was performed to determine the percent difference between FEA results for cylinders with oblique holes and photoelastic results for plates with oblique holes, both subjected to tensile loading. Tension loads were applied to models with geometries that most closely matched the thickness to hole diameter ratios included in the photoelastic study of Stanley and Day [5]. For the plates in which the applied load is parallel to the major axis of the ellipse at the hole surface, the thickness-to-hole diameter ratios included in Stanley and Day [5] were 1.33 and 2.00.

Cylinder geometries selected for comparison result in wall thickness to hole diameter ratios of 1.25 and 2.5. This corresponds to geometries with an inner cylinder diameter of 15 mm and a hole diameter of 1 mm or 2 mm. A uniform tension load was applied to the upper surface of the cylinder and the bottom surface was fully constrained in all six degrees of freedom.

The results of the finite element models are shown with the results of Stanley and Day [5] in Figure 4-2. The maximum percent difference is 11.67 %. This occurs at an obliquity angle of 60°. At 30° of obliquity, the percent difference in results is 9.87 %. Elsewhere, results are within 3.00 %.

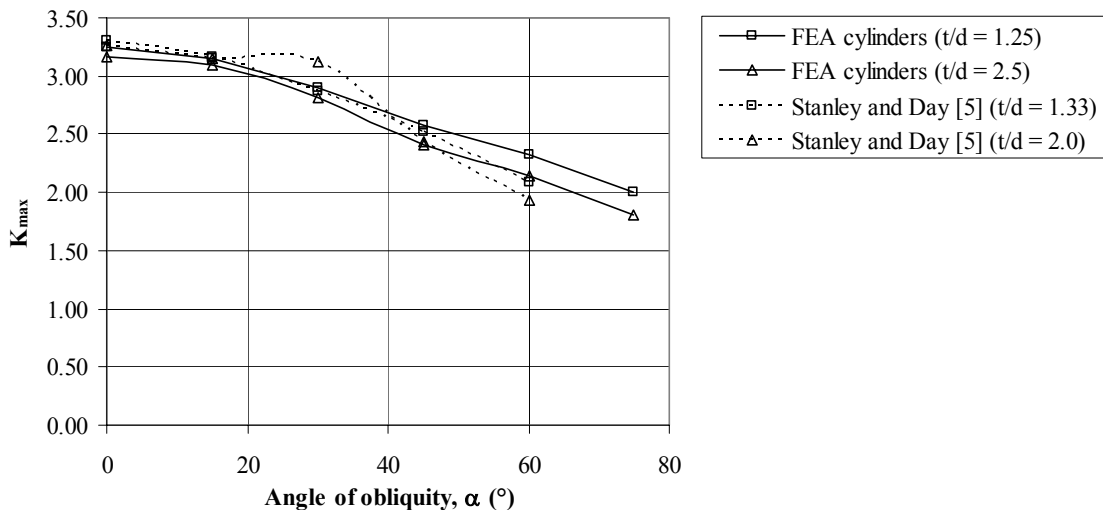
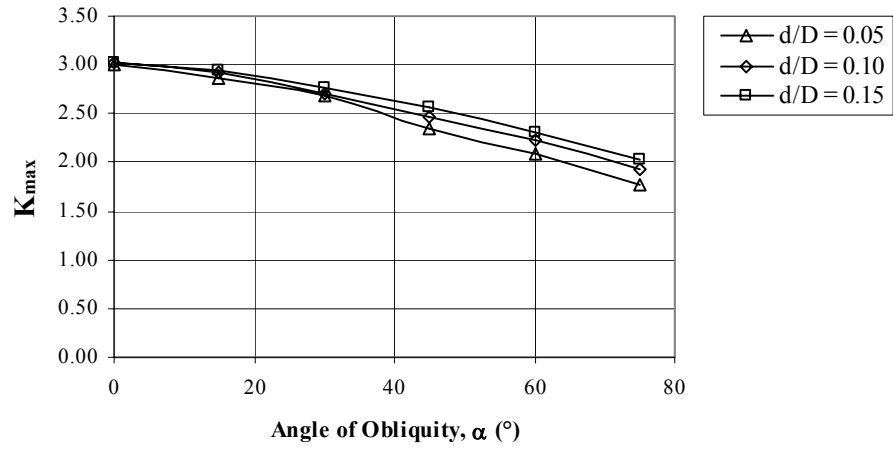


Figure 4-2 Comparison of results from FEA and Stanley and Day [5]

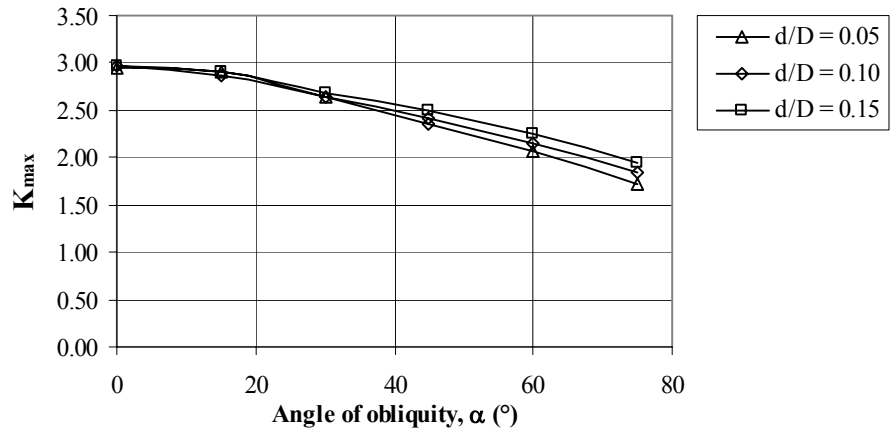
Angle of Obliquity, α

Figure 4-3 illustrates the relationship between obliquity angle and K_{max} for various d_i/D ratios. For every hole geometry in this study, K_{max} approaches 3.00 at $\alpha = 0$ and the value decreases as α increases. At a 60° obliquity angle, K_{max} is an average of 28% smaller than the value at 0°.

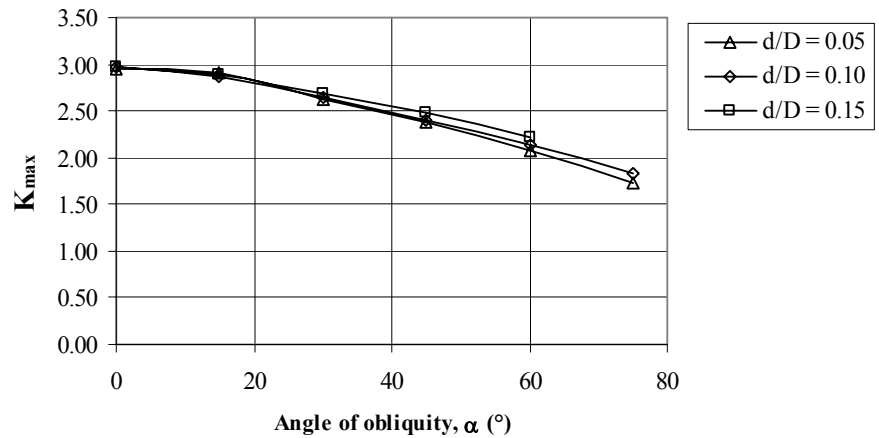
The relationship between K_{max} and α is similar for every hole diameter-to-outer cylinder diameter ratio and wall thickness (inversely proportional to the cylinder diameter)



(a)



(b)



(c)

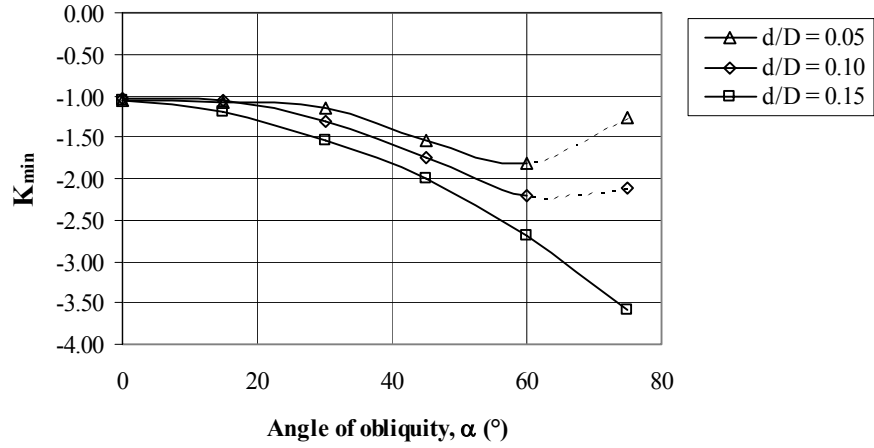
Figure 4-3 K_{max} plotted against α , (a) $d_i/D = 0.75$, (b) $d_i/D = 0.50$, (c) $d_i/D = 0.25$ ratio, d_i/D). A slightly larger variation in K_{max} values occurs when d_i/D is 0.75 (Figure 4-3a). This d_i/D ratio represents the thinnest wall.

K_{min} is plotted against α for various d_i/D ratios in Figure 4-4. Similar to the K_{max} results, more variation in the data occurs for the largest d_i/D ratio (Figure 4-4a). In all of these plots, K_{min} increases in magnitude as obliquity angle increases from 0° to 60° , but, for the smallest d_i/D ratio (i.e. the smallest hole diameter), K_{min} sharply decreases in magnitude as the angle of obliquity approaches 75° . This may be due to the combined effects of a large stress gradient near the K_{min} location for this extreme obliquity angle and non-uniform node placement. The node placement may not have captured the absolute minimum stress.

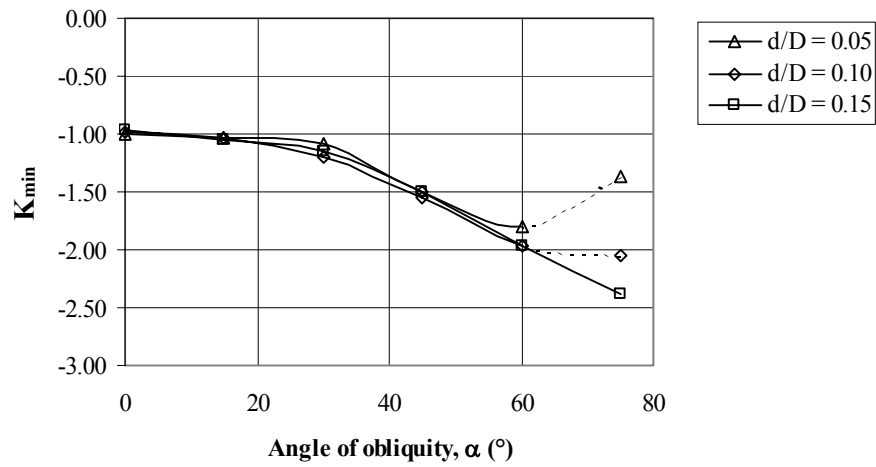
Hole Size Ratio, d/D

The variation in maximum stress concentration as d/D changes at $d_i/D = 0.75$ is plotted in Figure 4-4. Plots for other d_i/D ratios are similar. The plots demonstrate that K_{max} is not strongly dependent on d/D , especially at small obliquity angles. At larger obliquities, increasing d/D causes an increase in K_{max} . For an obliquity angle of 75° , there is a 12% increase in the maximum stress concentration factor as the hole diameter ratio increases from 0.05 to 0.15.

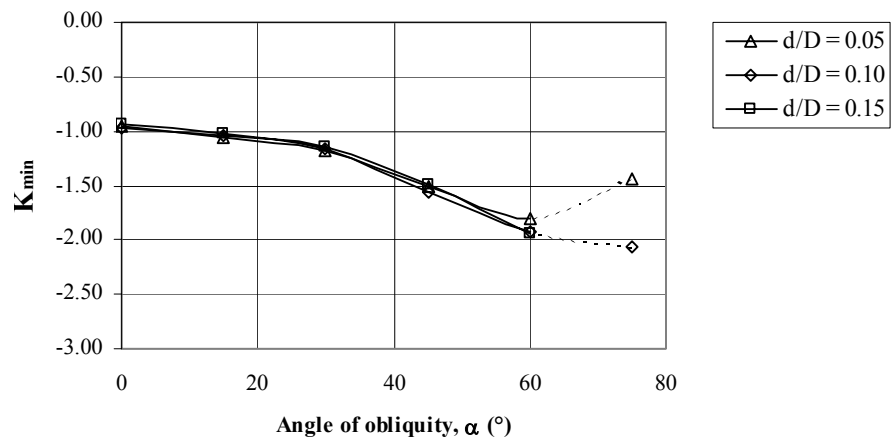
The relationship between K_{min} and d/D is illustrated in Figure 4-5 at $d_i/D = 0.75$. This relationship is stronger than the relationship between K_{max} and d/D . As d/D increases, K_{min} decreases. The rate of decrease is larger for larger angles of obliquity. At a 75° angle of obliquity, the rate of decrease in K_{min} values is very large, but the values



(a)



(b)



(c)

Figure 4-4 K_{min} plotted against α , (a) $d_i/D = 0.75$, (b) $d_i/D = 0.50$, (c) $d_i/D = 0.25$

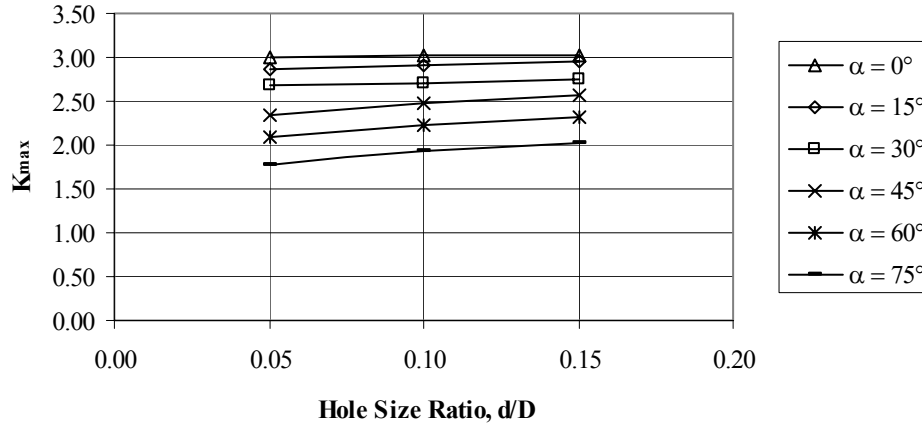


Figure 4-5 K_{max} plotted against hole size ratio, d/D , at $d_i/D = 0.75$

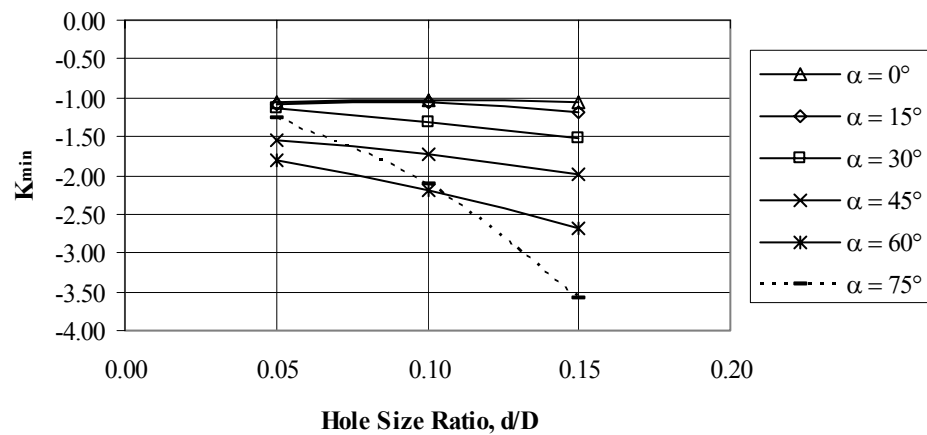


Figure 4-6 K_{min} plotted against hole size ratio, d/D , at $d_i/D = 0.75$

are not in keeping with the other values on the chart. This may be due to the previously discussed large stress gradient at the K_{min} location and the non-uniform stress gradient for models with a 75° angle of obliquity.

Cylinder Diameter Ratio, d_i/D

Figure 4-7 illustrates the relationship between K_{max} and the cylinder diameter ratio for various obliquity angles at $d/D = 0.10$. The relationship at other d/D ratios is very similar. The chart indicates that K_{max} is not dependent on wall thickness. A comparison of this chart with Figure 4-5 reveals that K_{max} is more dependant on d/D than d_i/D .

A plot of K_{min} versus the d_i/D ratio is shown in Figure 4-8 for a d/D ratio of 0.10. The behavior of these results is somewhat similar to the behavior of the K_{max} results, but

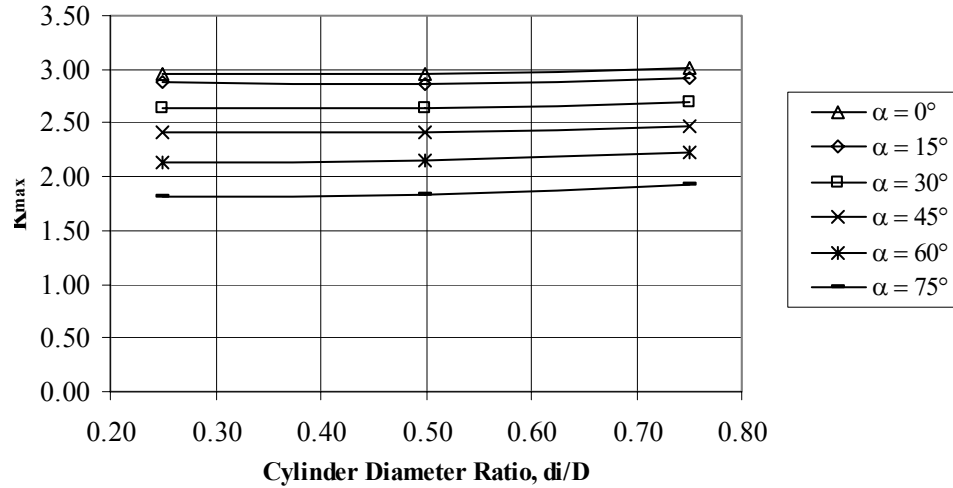


Figure 4-7 K_{max} plotted against d_i/D for various α at $d/D = 0.10$

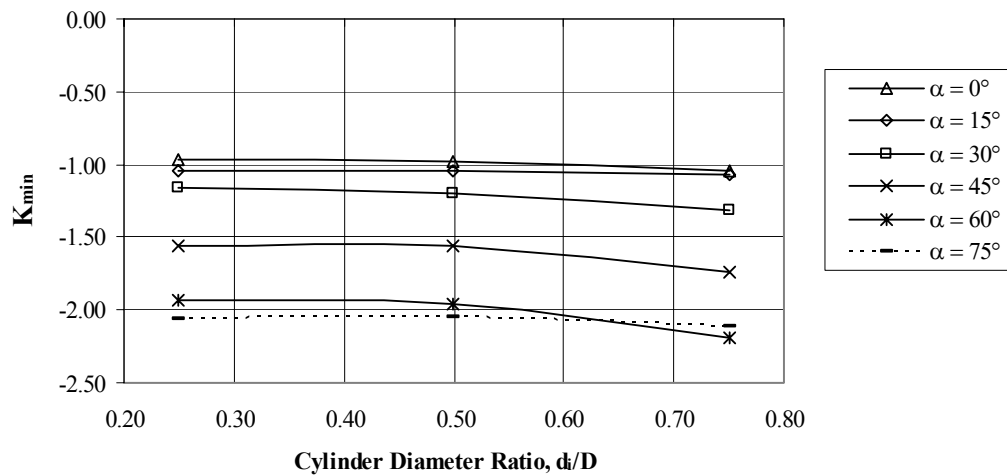
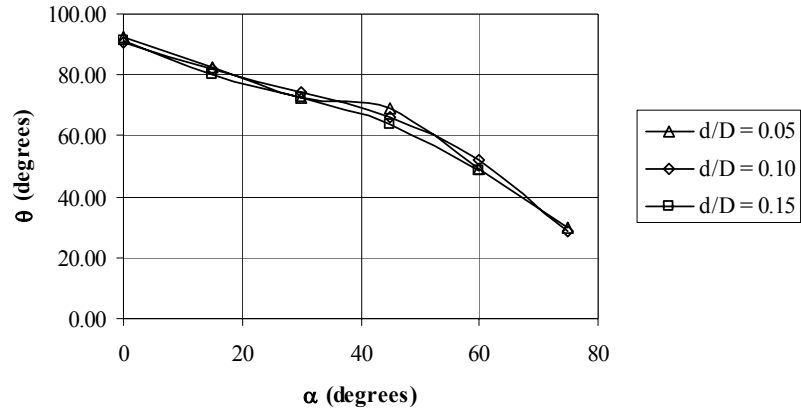


Figure 4-8 K_{min} plotted against d_i/D for various α at $d/D = 0.10$

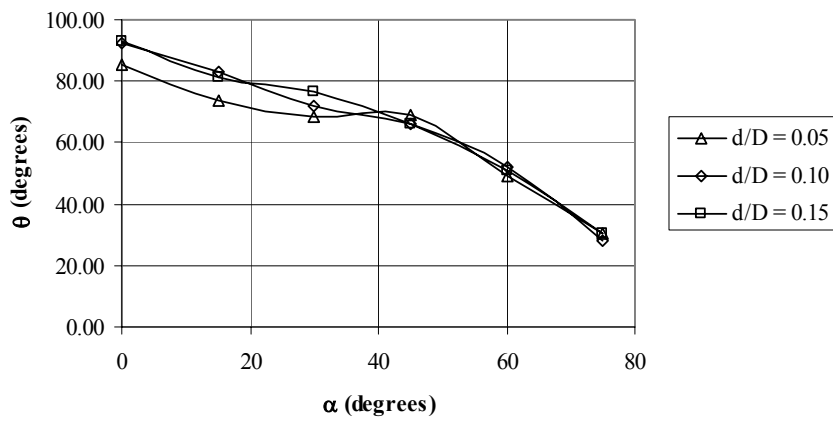
the wall thickness tends to have a stronger influence on K_{min} . As the wall thickness decreases (i.e. d_i/D increases), K_{min} decreases 14%. This trend occurs for every obliquity angle, indicating that the effect of the wall thickness on K_{min} is not influenced by the obliquity angle.

Angular Location of Maximum Stress, θ

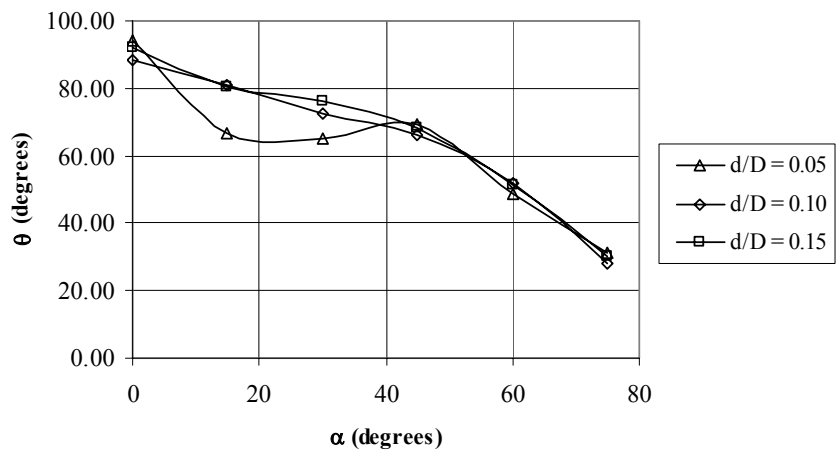
The effect of α on the angular location of K_{max} in the hole is illustrated in Figure 4-9 for each diameter ratio. The angular location is plotted in terms of θ , the angle around the hole in the plane perpendicular to the hole axis. This angle is defined from the



(a)



(b)



(c)

Figure 4-9 Angular location of K_{max} , θ , plotted against α
 (a) $d_i/D = 0.25$, (b) $d_i/D = 0.50$, (c) $d_i/D = 0.75$

point in the hole furthest from the direction of the applied load. The absolute value of each angular location is plotted for clarity.

In general, as α increases from 0° to 75° , θ shifts from 90° toward 30° . For the smallest d/D ratio, 0.05, K_{max} tends to plateau to 70° between 15° and 45° of obliquity. The effect is present in all cylinders, but is most pronounced for the thinnest cylinder, i.e. at $d_i/D = 0.75$.

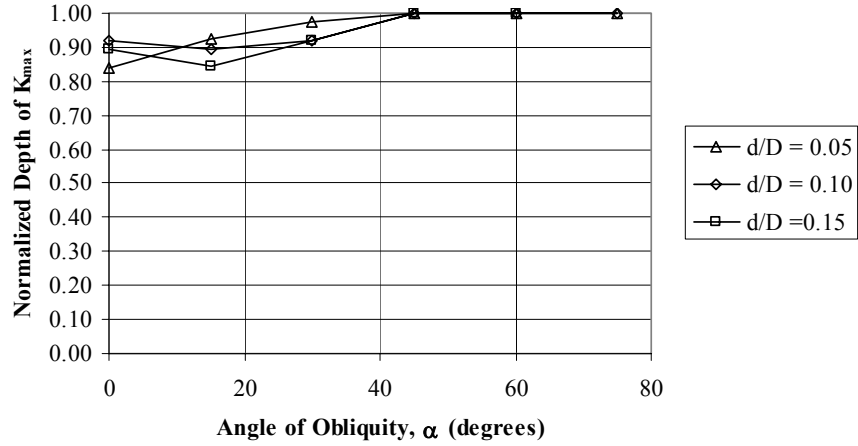
Depth of Maximum Stress in Hole, h

To provide a direct comparison of the position of maximum stress for all thicknesses, the radial locations reported in Table 4-1 have been normalized. The normalized depth of maximum stress in the hole, h , is determined using the following formula, which is a ratio of the distance of the maximum stress as measured from the mid-plane, to half of the wall thickness:

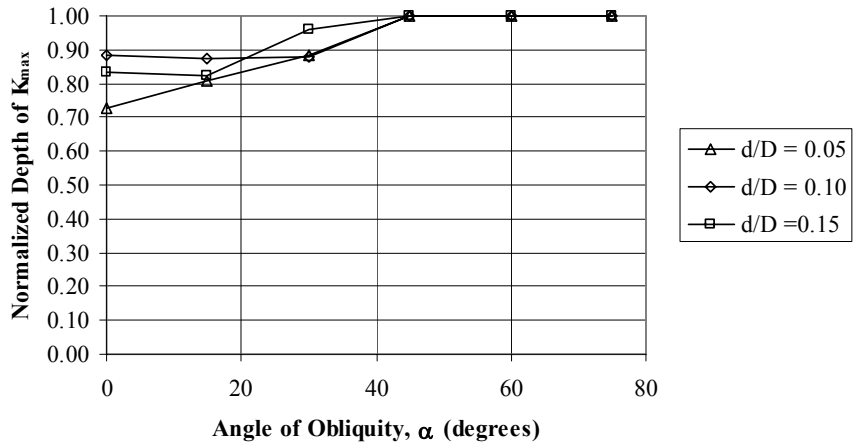
$$h = \frac{4r - D - d_i}{D - d_i}$$

Normalized depth values of 0.00 and 1.00 represent the mid-plane of the hole and the surface of the cylinder, respectively.

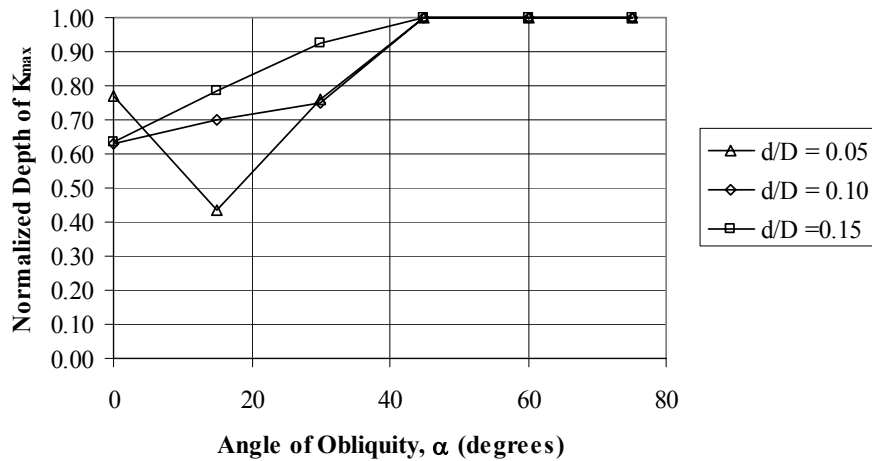
Figure 4-10 illustrates the relationship between the normalized distance of K_{max} from the mid-plane and the angle of obliquity for various cylinder diameter ratios. As the angle of obliquity is increased, the K_{max} shifts rapidly toward the plate surface. K_{max} is located on the cylinder surface for all obliquity angles over 45° . The absolute value of the normalized depth was used to generate the plots, so the surface indicated by the value '1.00' may be either the inner or outer surface.



(a)



(b)



(c)

Figure 4-10 Normalized depth of K_{max} in the hole interior plotted against α (a) $d_i/D = 0.25$, (b) $d_i/D = 0.50$, (c) $d_i/D = 0.75$ degrees (see Figure 3.1).

Angle of Neutral Axis, ψ

To compare the results of this study to the stress concentration factor in the canine tibia, a modification to the results would be necessary. The force couple applied to generate all previous results was oriented such that the neutral axis is at $\psi = 0$. This is the most critical bending load case for this geometry, resulting in the largest maximum principal stresses. The physiologic loading of the canine tibia, however, is such that the neutral axis is closer to $\psi = 180^\circ$. This loading results in compression in the region of the cylinder surrounding the hole.

Selected models, chosen for parameters that most closely matched that of the canine tibia, were subjected to a bending moment with a neutral axis at $\psi = 180^\circ$ (see Figure 3.1). At the nutrient foramen, the canine tibia has an outside wall diameter of approximately 15 millimeters, a wall thickness of approximately 2 millimeters, a nutrient foramen diameter of less than 2 millimeters, and an obliquity angle that approaches 75° . The models selected for the loading comparison were 47, 48, 50, and 51 (see Table 3.1).

Results indicate that a simple modification of the $\psi = 0^\circ$ results yield results comparable to canine tibia stress concentration factors. For each model, the maximum principal stress at $\psi = 180^\circ$ is equivalent to the absolute value of the minimum principal stress at $\psi = 0^\circ$. Similarly, the absolute value of the minimum principal stress at $\psi = 180^\circ$ is equivalent to the maximum principal stress at $\psi = 0^\circ$. So, to compare these results to the maximum stress concentration factor in the canine tibia, it would be necessary to choose the absolute value of the minimum stress concentration factor for the most applicable geometry.

CHAPTER 5 DISCUSSION

Angle of Obliquity, α

A photoelastic study performed by Stanley and Day [5] lists results for flat plates with oblique holes subjected to uniform uniaxial tension parallel to the major axis of the ellipse created on the hole surface by the oblique hole (similar to the orientation of the hole in this study). The relationship between K_{max} and α illustrated in Figure 4-3 is consistent with the trends reported by Stanley and Day [5], which show that, for this load orientation, an increase in hole obliquity results in a decrease in the maximum stress concentration factor. As the angle of obliquity increases, the hole in the cylinder surface elongates. Results in Pilkey [2] indicate that elongating a hole in this direction in a plate in tension has the effect of reducing the stress concentration factor.

As obliquity increases, K_{max} decreases more in a flat plate in tension than in a cylinder in bending. This effect is due primarily to the geometry of the specimen, rather than the difference in loading. In the work performed by Stanley and Day [5], the maximum stress concentration factor at 60° is approximately 40 % smaller than the value at 0° . For cylinders in bending included in the current study, K_{max} decreases 28 % when α is varied from 0° to 60° . Cylinders subjected to tensile loading, which were compared to plates in tension in Figure 4-2, result in a K_{max} decrease of 28 % between $\alpha = 0^\circ$ and $\alpha = 60^\circ$.

As the angle of obliquity increases, minimum stress concentration factors increase in magnitude (see Figure 4-4). The aspect ratio of the ellipse created on the cylinder

surface also increases as obliquity increases. The minimum principal stress is located near the major axis of the ellipse. At this location, the radius of curvature decreases. Results indicate that decreasing the radius of curvature causes an increase in the stress gradient, which, in turn, decreases the area over which the stress is distributed. This effect contributes toward increasing the minimum stress concentration factor as obliquity angle increases. Minimum stress concentration factors were rarely reported in prior work on oblique holes in flat plates with uniaxial tension, so the results of this study supply new information to this area of research.

The sharp decrease in magnitude of K_{min} values in Figure 4-4 for small holes with a 75° angle of obliquity may be attributed to the mesh. An extremely high stress gradient was observed near the location of minimum stress for the smallest hole diameter and the largest hole obliquity. Non-uniform node placement combined with a large stress gradient decreases the probability that a node will be located precisely at the minimum stress location. This is especially important to consider when the stress changes drastically over a small geometric area. The precision with which accurate maximum and minimum stress values can be obtained in this region is influenced by the element size.

Hole Size Ratio, d/D

The relationship between maximum stress concentration factor and the hole size ratio, d/D , as shown in Figure 4-5, is comparable to the relationship developed in Jessop et al. [8] for cylinders with transverse holes in bending. As the hole size ratio increases, the maximum stress concentration factor increases slightly. This is expected, since increasing the diameter of the hole would increase the cross sectional area of the discontinuity, which would increase the stress concentration. A graphical comparison of

the finite element results to the photoelastic results in Jessop et al. [8] is included in Figure 4-1. A comparison revealed an 8.2 % difference in results.

Cylinder Diameter Ratio, d_i/D

The behavior of the maximum stress concentration factor as the cylinder diameter ratio is varied is also comparable to the results of Jessop et al. [8], which states that the effect of d_i/D on the maximum stress concentration factor for a cylinder in bending is not as great as the effect of varying d/D . This indicates that the thickness of the cylinder wall has less of an influence on the maximum stress concentration factor than does the hole diameter. Variations in the diameter or obliquity of the hole tend to have the greatest influence on the maximum stress concentration factor.

Angular Location of Maximum Stress, θ

As was shown in Figure 4-9, θ , the angular location of maximum stress, shifts from 90° toward 30° as the angle of obliquity increases from 0° to 75° . A similar trend was documented in Stanley and Day [5] for a flat plate in uniaxial tension with an oblique hole orientation similar to the orientation of holes in this study. In their photoelastic study, Stanley and Day reported a maximum stress located at 90° for every hole except one [5]. At a 60° obliquity and a thickness-to-hole diameter ratio of 2.59 (the largest ratio reported), maximum stress was located at $\theta = 60^\circ$.

The slices used in the photoelastic study of Stanley and Day [5] were located every 30° around the circumference of the hole, so the accuracy of the locations reported is limited. A trend of decreasing angular location of maximum stress concentration factor may have been present for all thickness-to-hole diameter ratios, but was most pronounced when the thickness-to-hole diameter ratio was the largest.

Depth of Maximum Stress in Hole, h

The plots in Figure 4-10 indicate that the position of K_{max} shifts toward the plate surface as the angle of obliquity increases. This is comparable to the behavior noted in Dulieu-Barton and Quinn [6], in which K_{max} position data were compiled from Stanley and Day [5], McKenzie and White [12], and Leven [13]. All data were from investigations of flat plates with oblique holes loaded in tension parallel to the minor axis of the ellipse (perpendicular to the orientation of holes in this study). Results showed that as the angle of obliquity increases from 0° to 60° , the maximum stress moves from the mid-plane to the plate surface. An additional plot in Dulieu-Barton and Quinn [6] shows that varying the angle of applied load from parallel to the minor axis of the ellipse to parallel to the major axis does little to alter the depth of maximum stress on the hole interior.

As the angle of obliquity increases, the location of maximum stress reaches the hole edge more rapidly in cylinders in bending than in flat plates in tension. In the cylinders in this study, the maximum stress is located on the hole edge for all obliquity angles over 45° . For flat plates loaded in tension, however, only holes with obliquity angles over 60° exhibit maximum stress located on the hole edge. This may be due to the applied bending load, which causes high tensile stresses to occur near the surface.

Angle of Neutral Axis, ψ

Results in Table 4-1 were generated using a force couple that results in tension on the region of the cylinder surrounding the hole ($\psi = 0^\circ$). Selected models with geometry similar to the canine tibia were loaded such that the region surrounding the hole is in compression. This corresponds to $\psi = 180^\circ$. A comparison of results at different ψ

angles revealed that the magnitude of maximum principal stress at $\psi = 180$ is equal to the magnitude of minimum principal stress at $\psi = 0^\circ$. To use these results as a comparison tool to help quantify mechanical improvements in the canine tibia, the absolute value of the minimum stress concentration factor as reported should be compared to the maximum stress concentration factor in the canine tibia.

CHAPTER 6 CONCLUSIONS

This study provides a detailed discussion of stress concentration factors in cylinders with either oblique or transverse holes in bending. Results demonstrate a strong relationship between maximum stress concentration factor and the angle of obliquity. For the loading scheme studied, as the obliquity increases, the maximum stress concentration factor decreases.

A weak dependency exists between the maximum stress concentration factor and the hole diameter-to-outer cylinder diameter ratio. An increase in this ratio tends to result in a slight increase in the maximum stress concentration factor. For an obliquity angle of 75° , there is a 12% increase in the maximum stress concentration factor as the hole diameter ratio increases from 0.05 to 0.15.

The results compare well to previous work. The changes in the maximum stress concentration factor with respect to the angle of obliquity, wall thickness, and hole diameter are supported by the trends of prior studies. The angular location and depth of the maximum stress concentration factor in the hole are also in keeping with earlier findings. As compared to flat plates in tension, though, cylinders in bending tend to result in maximum stress locations that shift more rapidly toward the acute intersection of the hole with the plate as the angle of obliquity increases. In addition, maximum stress concentration factors for plates in tension decrease more than corresponding factors in cylinders in either bending or tension as the obliquity angle is increased from 0° to 60° .

Minimum stress concentration factors at any angle of obliquity and all data generated from a 75° angle of obliquity have been largely overlooked in previous work, but results are not unexpected. As the obliquity increases from 0° to 60°, the magnitude of minimum stress concentration factors tends to increase as the magnitude of maximum stress concentration factors decreases. This may be due to a change in the radius of curvature, which decreases at the location of minimum stress as the obliquity increases. The magnitude and location of maximum stress concentration factors at a 75° obliquity angle, similarly, are consistent with values at other obliquity angles.

Somewhat unexpected results, however, occur for the minimum stress concentration factors reported at a 75° angle of obliquity. Non-uniform node placement is responsible for these deviations. At this obliquity angle, the minimum stress occurs near a large stress gradient and the location of minimum stress does not coincide with a node, so the reported stress may be much larger than the absolute minimum, although the two are in close proximity.

Data generated by this project may be compared to stress concentration values associated with the nutrient foramen in the canine tibia. The canine tibia is loaded in bending in the saggital plane such that the nutrient foramen is primarily in compression. The bending load applied in this study, however, would put the hole in tension. For directly comparable results, the absolute value of K_{min} from this report should be considered to be the maximum stress concentration factor.

To obtain stress concentration values for the canine tibia, a microstructural analysis of bone samples near the nutrient foramen would be performed to find approximate elastic constants at discrete locations. These values could then be used in a finite element

model to simulate the stiffness variations. Stress concentration factors in the canine tibia could then be established for comparison with values explored in detail in this report.

If, as expected, a stiffness gradient similar to that discovered around the equine third metacarpus nutrient foramen is present at the canine tibia foramen, the maximum stress concentration factor in bone would be lower than that in a homogeneous, isotropic structure. The results of this study provide comparison data that will help to quantify the ability of bone to reduce stress around geometric discontinuities.

LIST OF REFERENCES

- [1] Götzen N, Cross AR, Ifju PJ, Rapoff AJ. Understanding stress concentration about a nutrient foramen. *J Biomech* 2003; 36(10): 1511-1521.
- [2] Pilkey WD. Peterson's Stress Concentration Factors, 2nd Edition, John Wiley & Sons, New York, 1997.
- [3] Ellyin F, Lind NC, Sherbourne AN. Elastic stress field in a plate with a skew hole. *J Eng Mech-ASCE* 1966; 92: 1-10.
- [4] Ellyin F. Experimental study of oblique circular cylindrical apertures in plates. *Exp Mech* 1970; 10: 195-202.
- [5] Stanley P, Day BV. Photoelastic investigation of stresses at an oblique hole in a thick flat plate under uniform uniaxial tension. *J Strain Anal Eng* 1990; 25(3): 157-175.
- [6] Dulieu-Barton JM, Quinn S. Thermoelastic stress analysis of oblique holes in flat plates. *Int J Mech Sci* 1999; 41: 527-546.
- [7] Daniel IM. Photoelastic analysis of stresses around oblique holes. *Exp Mech* 1970; 10: 467-473.
- [8] Jessop HT, Snell C, Allison IM. The stress concentration factors in cylindrical tubes with transverse cylindrical holes. *Aeronaut Q* 1959; 10: 326-344.
- [9] Tafreshi A, Thorpe TE. Numerical analysis of stresses at oblique holes in plates subjected to tension and bending. *J Strain Anal Eng* 1995; 30(4): 317-323.
- [10] Cook R.D, Malkus DS, Plesha ME, Witt RJ. Concepts and Applications of Finite Element Analysis, 4th Edition, John Wiley & Sons, New York, 2002.
- [11] I-DEAS 9.0 Structural Dynamics Research Corporation. Online Help Bookshelf, Simulation: Element Library, 2001.
- [12] McKenzie HW, White DJ. Stress concentration caused by an oblique round hole in a flat plate under uniaxial tension. *J Strain Anal Eng* 1968; 3(2): 98-102.
- [13] Leven MM. Photoelastic determination of the stresses at oblique openings in plates and shells. *Welding Research Council Bulletin* 1970; 153: 52-80.

BIOGRAPHICAL SKETCH

Susan Andrea Mathison was born on September 30, 1974, in Huntsville, Alabama, to Julian and Sue Mathison. She has one older brother, Michael. She attended Huntsville High School from 1988 to 1992, where she was a member of the concert band and co-captain of the color guard. After graduation, she moved to Knoxville, Tennessee, and became a student in radiological engineering at the University of Tennessee. It was there that she met Guy Grover, another student in the same department. They married on August 6, 1994, in Huntsville and she changed her name to Susan Mathison Grover. A year later, she decided to switch her major. She graduated in May 1997 with a Bachelor of Science degree in engineering science and mechanics with a concentration in biomedical engineering.

On June 23, 1997, she joined USBI, Inc., a division of United Technologies, performing structural analyses of re-usable Space Shuttle Solid Rocket Booster hardware. She worked there for 5 years, before resigning in January 2003 to attend the University of Florida full-time to pursue a Master of Science degree in biomedical engineering. Since then, she has been working in the Applied Biomechanics Laboratory at UF. She is also currently working as an Intern at Regeneration Technologies, Inc., in Alachua, Florida. After graduation, she plans to find a job in the medical device industry.